ROYAL SOCIETY
OF CHEMISTRY

PAPER

Check for updates

Prussian blue coated with reduced graphene oxide as high-performance cathode for lithium–Sulfur batteries†

Minghua Chen, ⓘ * Zhanpeng Zhang, Xiaoxue Liu,* Yu Li, Yuqing Wang, He Fan, Xinqi Liang* and Qingguo Chen

Lithium–sulfur (Li–S) batteries with their outstanding theoretical energy density are strongly considered to take over the post-lithium ion battery era; however, they are limited by sluggish reaction kinetics and the severe shuttling of soluble lithium polysulfides. Prussian blue analogues (PBs) have demonstrated their efficiency in hindering the shuttle effects as host materials of sulfur; unfortunately, they show an inferior electronic conductivity, exhibiting considerable lifespan but poor rate performance. Herein, we rationally designed a PB@reduced graphene oxide as the host material for sulfur (S@PB@rGO) hybrids *via* a facile liquid diffusion and physical absorption method, in which the sulfur was integrated into $Na_2Co[Fe(CN)_6]$ and rGO framework. When employed as a cathode, the as-prepared hybrid exhibited excellent rate ability (719 mA h g^{-1} at 1C) and cycle stability (918 mA h g^{-1} at 0.5C after 100 cycles). The improved electrochemical performance was attributed to the synergetic effect of PB and conductive rGO, which not only enhanced the physisorption of polysulfides but also provided a conductive skeleton to ensure rapid charge transfer kinetics, achieving high energy/power outputs and considerable lifespan simultaneously. This study may offer a new method manufacturing high performance Li–S batteries.

1. Introduction

The increasing demand for the widespread application of renewable and sustainable energy triggered the rapid development of low-cost, high energy/power density electrochemical energy storage devices to cope with the climate change crisis.[1–4] The energy storage devices can be commonly categorized into two categories: supercapacitors (SCs) and secondary batteries.[5–10] Among them, lithium–sulfur (Li–S) batteries, a powerful and promising category of sustainable rechargeable batteries, have been attracting increasing attention owing to their high capacity, low cost, and environmental friendliness.[11,12] In addition, the high theoretical energy density (2600 W h kg^{-1}) and theoretical specific capacity (1675 mA h g^{-1}) of Li–S batteries are much higher than those of other solid cathode materials.[13] In addition to the high theoretical energy density,[14] sulfur resources are abundant and environmentally benign.[15] However, the Li–S batteries have numerous drawbacks including the inferior conductivity of sulfur, volume fluctuation,[16] and the formation of soluble intermediate polysulfides during the redox process shuttle between electrodes (shuttling effect),[17] resulting in poor cycle stability, low coulombic efficiency and rapid degradation of capacity.[18] Up to now, these problems could not be completely eliminated.

It is known that sulfur embedded into highly conductive and robust nanostructured host materials, such as graphene,[19] nanostructured carbon,[20–22] polyaniline nanotubes[5] and metal–organic frameworks (MOFs),[23] can effectively mitigate the shuttle effect and sluggish reaction kinetics, thus improving the electrochemical performance of Li–S batteries. Recently, Wang *et al.*[24] reported that poly(ethylene glycol) (PEG) and graphene-coated sulfur particles can effectively inhibit the volume expansion of sulfur particles during the charge/discharge process. The resulting graphene–sulfur composite material showed specific capacity up to ~600 mA h g^{-1} at 100 cycles. Zhong *et al.*[25] demonstrated an integrated composite scaffold based on porous carbon fiber/vanadium nitride array composite material as the sulfur host, which showed enhanced rate capability. Obviously, the sulfur loading method has an important effect on the electrochemical properties of sulfur-containing composites. The selection of a suitable preparation process is of great significance to ensure the high sulfur loading and sulfur utilization of composites after long-term recycling. Nevertheless, the complex preparation process of the above-mentioned materials is difficult to meet the practical applications of this technique. Therefore, the preparation of sulfur-containing composites must be simple and feasible, while

Key Laboratory of Engineering Dielectric and Applications (Ministry of Education), Harbin University of Science and Technology, Harbin 150080, P. R. China. E-mail: mhchen@hrbust.edu.cn

† Electronic supplementary information (ESI) available. See DOI: 10.1039/d0ra04901h

selecting suitable hosts.[26] Prussian blue and its analogues (PBAs) have become the cathode materials for lithium-ion batteries, sodium-ion batteries and Li–S batteries[27] due to their good structure stability, low-cost and eco-friendly nature. Prussian blue has a crystal structure similar to MOFs composed of transition metal ions and organic linkers through covalent coordination linkages, showing high specific surface areas, ultra-high porosities, and well-defined pore structures. These unique structural superiorities endow PBAs with an impressive adsorption capacity analogous to that of activated carbon, and it is relatively easy to obtain. It can adsorb sulfur and polysulfide on the surface, and act as a host of sulfur. Although Prussian blue has been widely used in the field of energy,[28] it has rarely been investigated for Li–S batteries.

Herein, we report Prussian blue analogue-Na$_2$CoFe(CN)$_6$-coated reduced graphene oxide composited as a sulfur host material (S@PB@rGO) for high-performance Li–S batteries via a facile liquid diffusion and physical absorption method.[29] The advanced composite design offers the following advantages. (i) PB has an adsorption property similar to that of activated carbon, which can adsorb sulfur and polysulfide on the surface and act as a host of sulfur. (ii) During the charge and discharge process, the large framework structure of PB can accommodate the volume expansion of the active material and provide a larger transmission channel for the insertion/extraction of Li$^+$, leading to exceptionally high cycling stability. (iii) After combining with rGO,[15] it can be used as a physical confinement for the polysulfide shuttle effect. In addition, rGO has polar sites that can chemically adsorb long chain polysulfides.[2] As a result, the S@PB@rGO composite electrode shows remarkable cycling performance and improved rate performance.

2. Experimental section

2.1 Preparation of Na$_2$Co[Fe(CN)$_6$]

The Na$_2$Co[Fe(CN)$_6$] powder was synthesized via co-precipitation. First, 1 mmol Na$_4$Fe(CN)$_6$·10H$_2$O and 14 g polyvinyl pyrrolidone (PVP, Sigma-Aldrich, MW = ~40 000) were vigorously stirred in HCl solution (0.1 M, 100 ml). 5 mmol CoCl$_2$ was dissolved into 100 ml DI water. Then, this solution was added dropwise to 100 ml of Na$_4$Fe(CN)$_6$/PVP solution for their coprecipitation reaction. After stirring for 1 h, the reaction solution was placed into an electric oven and heated at 80 °C for 12 h. The resulting precipitates were filtered, and washed three times with DI water and ethanol, and finally dried under vacuum at 80 °C for 12 h.

2.2 Preparation of S@Na$_2$Co[Fe(CN)$_6$]

The S@Na$_2$Co[Fe(CN)$_6$] composite was prepared by dissolving Na$_2$Co[Fe(CN)$_6$] powder and sulfur in a ratio of 1 : 4 in carbon disulfide (CS$_2$, Sigma-Aldrich, ≥99%) solution. The mixture was vigorously stirred, and CS$_2$ was evaporated at 40 °C. The S@Na$_2$Co[Fe(CN)$_6$] multi-composites were filtered and washed with DI water and ethanol, and finally dried at 80 °C for 12 h.

2.3 Preparation of GO

GO was prepared via a modified Hummers' method from natural flake graphite powder. Briefly, 5 g of graphite was mixed with 300 ml of concentrated H$_2$SO$_4$ in an ice bath for 1 h. 10 g of KMnO$_4$ was then added into the above solution slowly under continuous stirring. The mixture was then kept at 90 °C for 4 h, washed with 5 wt% HCl and DI water, and the GO solution was obtained.

2.4 Preparation of S@Na$_2$Co[Fe(CN)$_6$]@rGO

1 ml GO aqueous suspension was diluted to 1.0 mg ml^{-1} with distilled water, and then sonicated for 1 h. S@Na$_2$Co[Fe(CN)$_6$] power was added into the rGO homogeneous aqueous. After stirring for 12 h, the S@Na$_2$Co[Fe(CN)$_6$]@rGO composite was washed with DI water and freeze-dried. The preparation procedure of S@rGO is mixing sulfur powder with a rGO solution directly, followed by washing and drying.

2.5 Characterizations

The crystal structure of the samples was determined via X-ray powder diffraction (XRD, Philips PC-APD) with Cu Kα radiation at 25 °C between 10 and 80°. The morphology of the samples was characterized via scanning electron microscopy (SEM, SU8000, Hitachi, Japan). Transmission electron microscopy (TEM, JEOL, Model JEM-2100) was used to investigate the lattice structure and surface feature of samples. TGA was conducted on a TGA/DSC 1 thermogravimetric analyzer (Mettler Toledo) in air from room temperature to 450 °C. Fourier transform infrared spectroscopy (FTIR) was performed on Perkin Elmer's Spectrum Two L160000A.

2.6 Electrochemical test

Electrochemical tests were performed by 2032 coin-type cells. The working electrodes were prepared by stirring the mixture of 80% of the active material, 10% of Super-P, and 10% of polyvinylidene fluoride (PVDF) in N-methyl-2-pyrrolidone (NMP). The slurry was spread evenly on an aluminum foil, and then dried at 80 °C under vacuum overnight. The as-prepared material as the cathode electrode, lithium foil as the anode electrode, Celgard 2300 as the separator, 1 M lithium bis(trifluoromethanesulfonyl)imide (LiTFSI) dissolved in 1,3-dioxolane (DOL) and 1,2-dimethoxyethane (DME) (in a volume ratio of 1 : 1), and 1 wt% lithium nitrate (LiNO$_3$) as the electrolyte were assembled into an electrochemical cell. Galvanostatic charge/discharge performances were measured using a NEWARE CT-4008 battery test system. The capacity was calculated based on the mass of sulfur. Cyclic voltammetry (CV) and electrochemical impedance spectroscopy (EIS) measurements were performed using a CHI 660E electrochemistry workstation. CV measurements were tested in the potential range of 1.8–2.8 V (Li/Li$^+$). EIS measurements were carried on the frequency ranges from 100 kHz to 10 MHz by applying an AC signal of 5 mV. In order to verify the electrochemical performance of different samples, the sulfur load of each electrode was limited to 0.8 mg cm^{-2}.

3. Results and discussion

The schematic of the preparation process for S@PB@rGO is shown in Fig. 1a. The $Na_2Co[Fe(CN)_6]$ powder was synthesized by co-precipitation, and then S@PB was prepared by physical adsorption and coated with rGO. S@PB exhibits a uniform nano-cubic structure of about 200–300 nm, as can be seen in Fig. 1b and c. The surface of S@PB becomes rougher when a small amount of sulfur particles is attached, which indicates that most of the sulfur particles adhere to the surface of PB. Fig. 1d shows the S@PB particles coated by ultra-thin rGO sheet. From the further enlarge image of Fig. 1e, we can clearly observe that the S@PB nanoparticles are tightly wrapped by ultra-thin graphene. For the in-depth investigation in the microstructure, the transmission electron microscopy (TEM) image of the S@PB@rGO composite is shown in Fig. 1f and e. The TEM image (Fig. 1f) shows a clear interface between the particle surface and the coating layer, and the inset shows the special shape of composite. The HRTEM image (Fig. 1g) of S@PB@rGO shows that the lattice fringe of sulfur is 0.217 nm. The sulfur particles are uniformly distributed.

Fig. 2a shows the XRD patterns of the S@PB and S@PB@rGO composite. Sulfur can be clearly identified by JCPDF: 83-2284.

Moreover, the sulfur in the two composites exhibits a good crystallinity and consistency. It indicates that sulfur is successfully integrated into the PB framework. As shown in Fig. 2b, thermogravimetric analysis (TGA) was performed to determine the sulfur content in the composite. The sulfur loading content of S@PB and S@PB@rGO composites was 74 wt% and 66 wt%, respectively. Raman spectrum for rGO and S are shown in Fig. 2c. The peaks at 150, 218, 435 and 470 cm^{-1} are indexed to sulfur, and the D band and G band belong to rGO, where the former represents the vibration of disordered carbon at the edge sites, and the latter shows the in-plane C–C band stretching vibration of graphitic carbon. It is defined that the ratio of I_D/I_G indicates the disordered degree of carbon materials. Here, the S@PB@rGO composite shows a I_D/I_G value of $I_D/I_G = 1.06$, suggesting that the coated rGO has fewer defects. The results of Raman spectra demonstrate that the rGO is successfully coated on the S@PB material. In order to fully explore the utilization of the PB frame structure, the loading of sulfur was achieved via a liquid diffusion process. S@PB and S@PB@rGO were characterized via FTIR, as shown in Fig. 2d, in which the peaks at 3420, 2970, 1612, 1400, 1047 cm^{-1} correspond to rGO. The peak of 598 cm^{-1} and 2082 cm^{-1} are identified as characteristic absorptions of the C–S bond and the CN
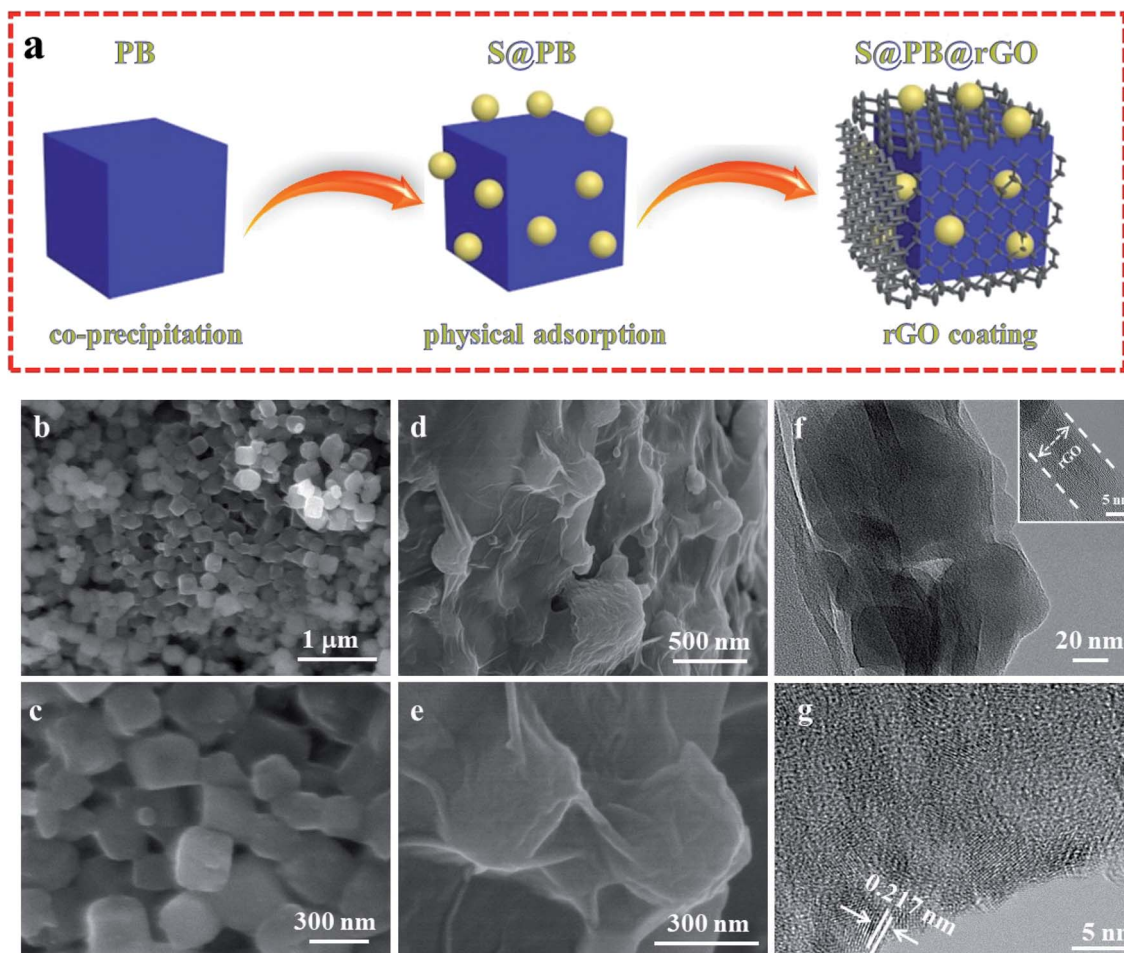

Fig. 1 (a) Schematic of the preparation process of S@PB@rGO. SEM images of (b and c) S@PB and (d and e) S@PB@rGO composites. (f and g) TEM and HRTEM images of S@PB@rGO composites.
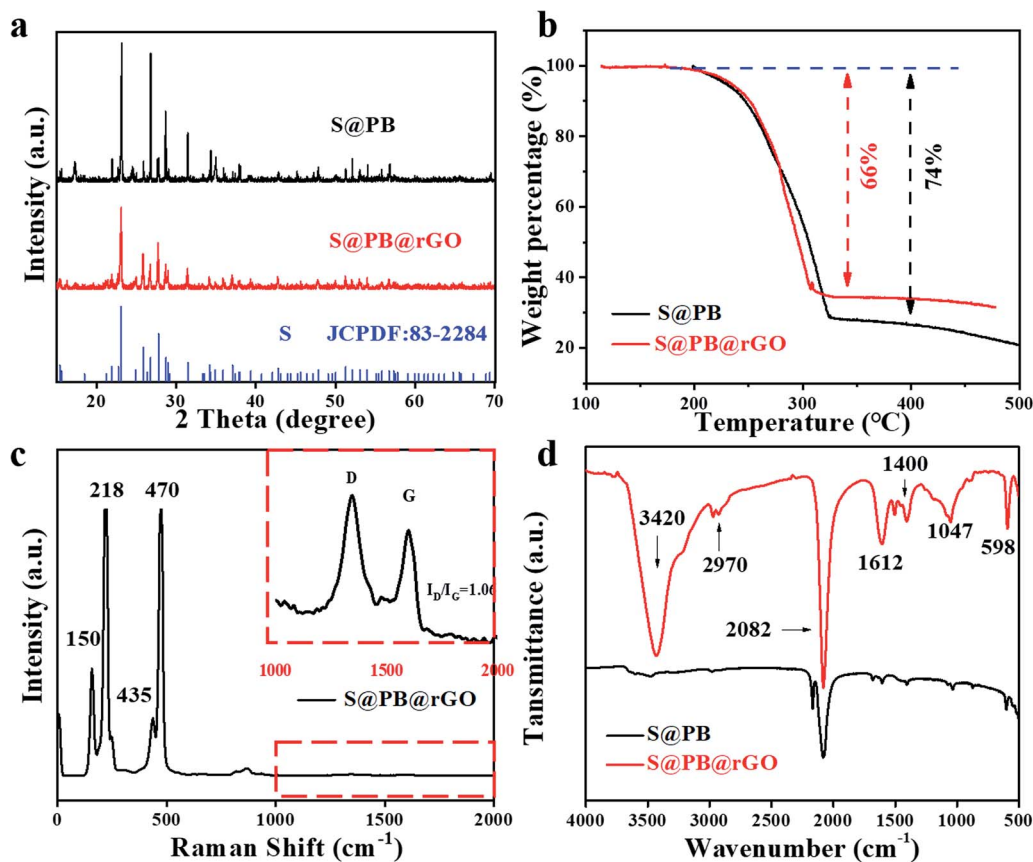
Fig. 2 (a) XRD patterns, (b) TGA curves measured in air, (c) Raman spectrum and (d) FTIR spectrum of the S@PB and S@PB@rGO composites.

stretching vibration of the hexacyanoferrate group, respectively. Both porosity and surface area are important indicators for sulfur host materials. According to the N_2 isothermal analysis (Fig. S1†), PB exhibits a high Brunauer–Emmett–Teller (BET) surface area of 59.376 with abundant mesoporous channels of ≈ 40 nm, as shown in Fig. S1† inset. The high porosity and large surface area of PB are favorable for offering more space for the loading of active materials.

The cyclic voltammetry curves of the S@PB@rGO electrode were recorded, as shown in Fig. 3a. There are two obvious cathode peaks at 2.0 V and 2.2 V due to the reduction of sulfur and the increase of polysulfides, one anode peak at 2.5 V is attributed to the conversion of polysulfides. It can be discerned from the good consistency of CV curves that the electrode is equipped with a commendable reversible ability and cycle stability. As shown in Fig. 3c, the cyclic stability test of S@PB@rGO and S@PB are obtained at the rate of 0.5C. The S@rGO performance is shown in Fig. S2,† while the longer cyclic stability tests of S@PB@rGO can be seen in Fig. S3.† The initial charge and discharge capacity of S@PB@rGO is 930 mA h g^{-1} and 918 mA h g^{-1}, respectively. In contrast, S@PB has a charge capacity of 618 mA h g^{-1} and a discharge capacity of 620 mA h g^{-1}. The S@rGO samples showed poor initial capacity and poor cyclic stability, possibly due to the uneven contact between S and rGO, and bulk sulfur polymerization. Notably, S@PB@rGO delivers high discharge capacity, which is

approximately 858 mA h g^{-1} at 0.5C, and the Coulomb efficiency maintains up to 97% during 100 cycles, while S@PB has a capacity of 520 mA h g^{-1}. It can be concluded that the rGO coating layer on the surface of the material can maintain the operation for a long period, thus improving the cycling stability and the capacity retention of the electrode. Moreover, as shown in Fig. 3d, S@PB@rGO has an obvious voltage plateau during the charge and discharge process, indicating that S@PB@rGO electrodes possess an infusive capacity retention.

As shown in Fig. 3e and S4,† at current rates of 0.1, 0.5, 1, 2 and 0.5C, the initial capacities of the S@PB@rGO electrode are 1163, 918, 721, 439 and 816 mA h g^{-1}, respectively. At the same current rates, the initial capacities of the S@PB electrode are 970, 621, 368, 122 and 600 mA h g^{-1} and that of the S@rGO electrode are 284, 141, 96 and 54 mA h g^{-1}, respectively. It shows that S@PB@rGO has better rate performance as compared with S@PB and S@rGO samples, demonstrating the advantage of the rGO coating. The charge and discharge curves of S@PB@rGO and S@rGO at different rates are shown in the Fig. 3f and S5,† respectively. The long charging and discharging voltage platform can be observed clearly in Fig. 3f, which indicates that the rGO coating and PB frame still possess synergistic effects in the shuttle effect of polysulfide under the condition of high rates. To further investigate the impact of rGO coating on performance, EIS test was performed. As shown in Fig. 3b, there are two similar impedance plots corresponding to the semicircle in the high
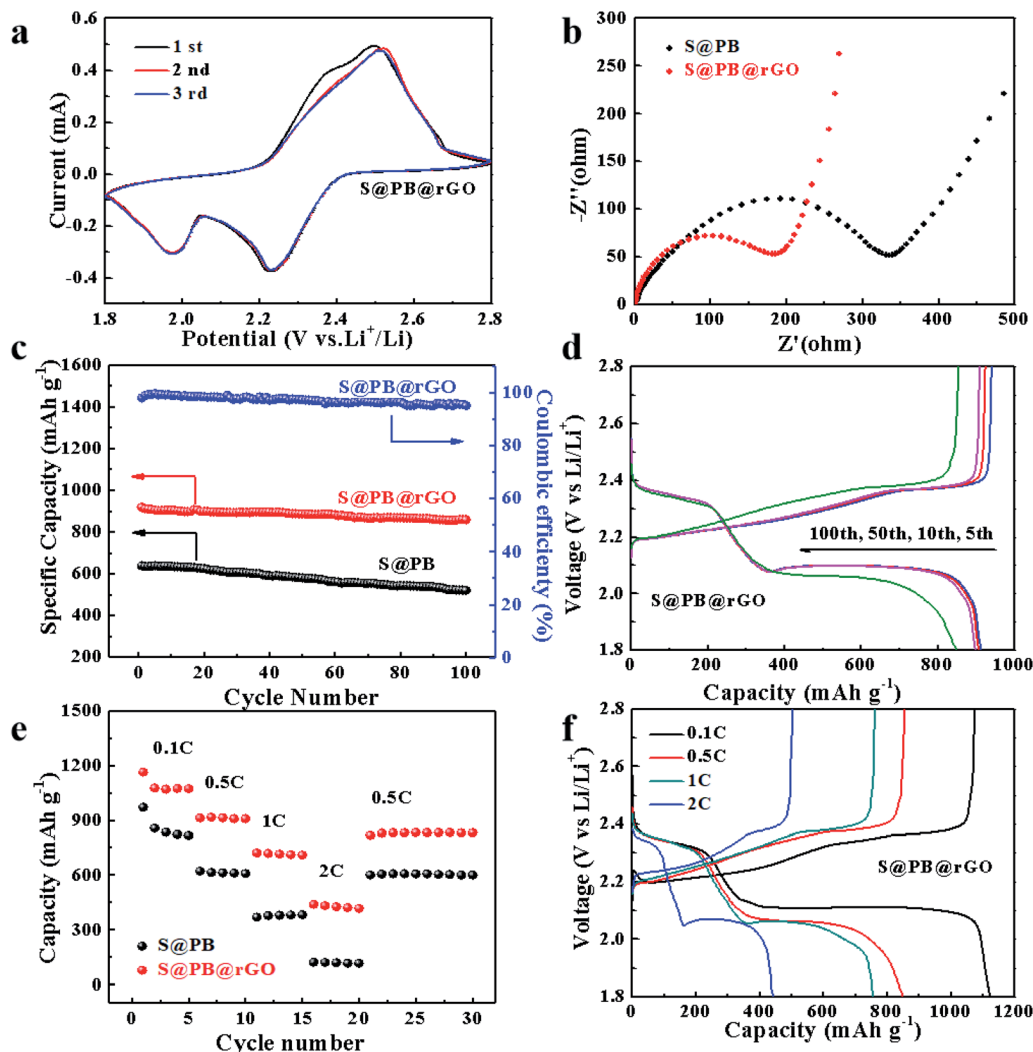
Fig. 3 (a) CV curves at the scan rate of 0.1 mV s^{-1} of S@PB@rGO electrodes. (b) EIS data of S@PB and S@PB@rGO electrodes. (c) Cycling stability of S@PB and S@PB@rGO electrodes at 0.5C rate for 100 cycles. (d) The discharge/charge curves at 0.5C of S@PB@rGO electrodes at 5th, 10th, 20th, 50th, and 100th. (e) Rate capability of S@PB and S@PB@rGO electrodes at various current densities. (f) The discharge/charge curves of S@PB@rGO electrodes at various current densities.

frequency and the slash line in the low frequency, respectively. The semicircle in the high frequency region relates to the diffusion of sulfur and polysulfides in the solid electrolyte interface (SEI). By comparing the high frequency regions of the two electrode materials, it can be seen that the rGO coating reduces the impedance and enhances the capacity of the materials.

In Fig. 4a–c, polysulfide solution is in bottle 1 and 3, polysulfide/PB mixed solution is in bottle 2 and polysulfide/PB@rGO mixed solution in bottle 4. Subsequently, it can be observed from the photos that the bottle 2 and 4 solutions become limpid gradually after 3 h of physical adsorption, which indicates that PB powder can not only assimilate the polysulfide but also can be turned into a host that polysulfide can settle down. Simultaneously, the PB@rGO composite can physically and chemically adsorb polysulfide in the electrolyte. As shown in Fig. 4d, PB has good sulfur storage abilities, and the large frame structure is easy to enter for Li$^+$/e$^-$. Coating with rGO increases

the conductivity of the material, and its layered structure does not hinder the transfer of charge, and prevents polysulfide from escaping from the host by physical restriction and chemisorption. In addition, the inclusion of sulfide and rGO layer in the crystal structure of PB can prevent the dissolution of polysulfide, reduce the shuttle effect, increase the interfacial charge transfer rate and sulfur utilization rate, leading to an excellent rate/cycling performance. Fig. S6a† indicates the CV curves of the cells employing S@PB@rGO as the cathode at various scan rates of 0.1, 0.2, and 0.3 mV s^{-1}. Based on the CV plots at various scanning rates, the Li ion diffusion coefficient (D_{Li^+}) could be calculated by the Randles–Sevick equation:[24]

$$I_{peak} = 268\,600 \times e^{1.5} \times area \times D_{Li^+}^{0.5} \times concn._{Li} \times rate^{0.5} \quad (1)$$

where I_{peak} is the current (A) of the peak, e is the number of electrons involved in the reaction, area is the electrode area (cm^2), concn.$_{Li}$ is the Li-ion concentration in the electrolyte (mol mL^{-1}),
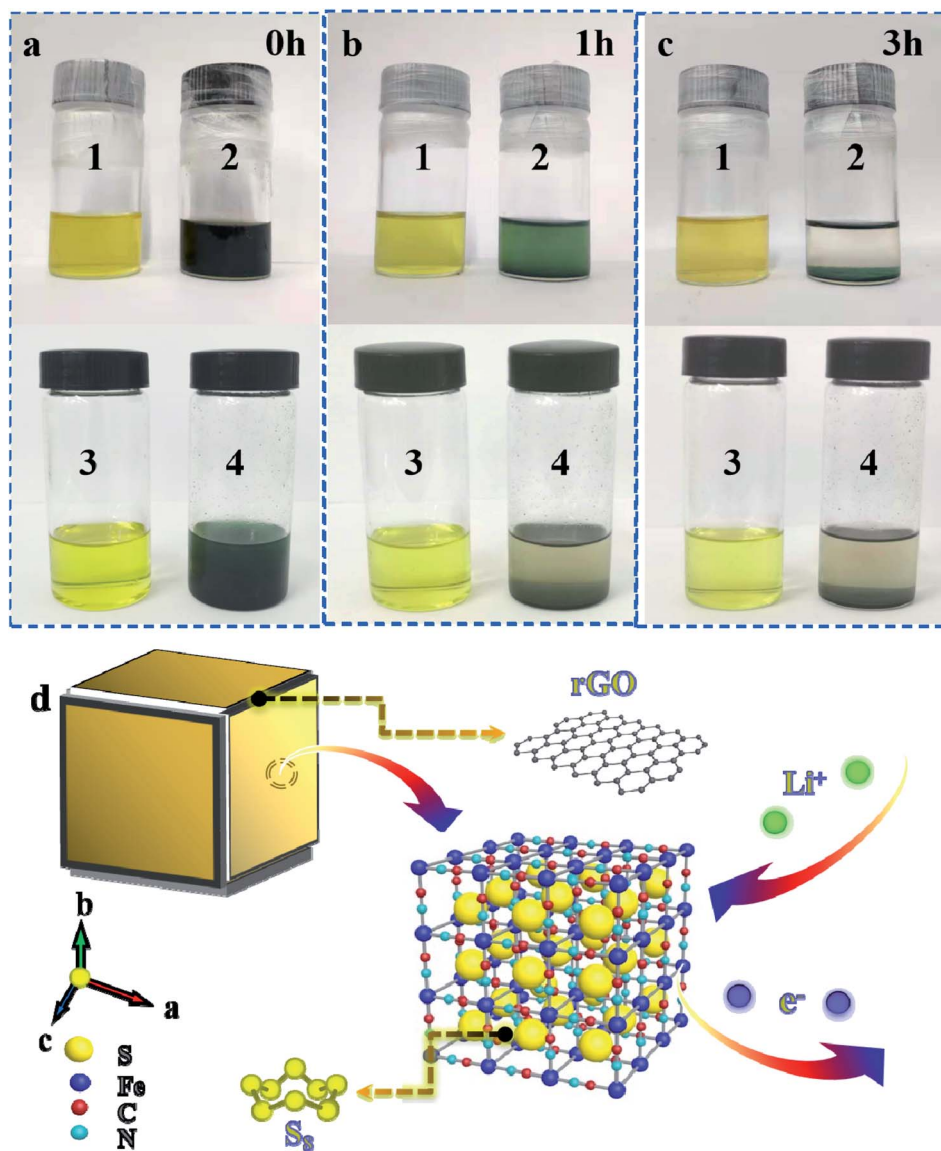
Fig. 4 (a–c) Photos of the PB and PB@rGO materials adsorbing polysulfide soaked into the electrolyte at 0 h, 1 h and 3 h, respectively. Bottles 1 and 3 are polysulfide solution, bottles 2, 4 are polysulfide/PB mixed solution and polysulfide/PB@rGO mixed solution; (d) illustration of the S@PB@rGO system in the discharge process.

and rate is the scanning rate in V s^{-1}. In order to calculate D_{Li^+}, we performed linear fitting for I_{peak} and rate$^{0.5}$ in CV plots under different scanning rates. The highly relevant linear relationship, as shown in Fig. S6b,† determines the diffusion coefficients (D_{Li^+}) at different CV voltage ranges: $D_{Li^+}(C_1) = 7.8 \times 10^{-9}$, $D_{Li^+}(C_2) = 2.02 \times 10^{-8}$, and $D_{Li^+}(A_1) = 4.27 \times 10^{-8}$ cm^2 s^{-1}.

4. Conclusion

In summary, we have demonstrated the rational preparation of advanced S@PB@rGO composites *via* a facile liquid diffusion and physical absorption method. The composites exhibited excellent rate performance and good cycling stability due to the physical adsorption and restriction of polysulfide in the PB open framework structure, and thus the active material loss

could be minimized. Moreover, the layered rGO not only physically hinders the diffusion of polysulfide but also provides chemically active sites to hinder the shuttle effect of polysulfides. This well-designed structure provides a low-cost and efficient way to fabricate high-performance cathode materials for the practical application of Li–S batteries.

Conflicts of interest

There are no conflicts to declare.

Acknowledgements

References

1 T. Wang, P. Shi, J. Chen, S. Cheng and H. Xiang, *J. Nanopart. Res.*, 2016, **18**, 1–9.

2 Z. Z. Yang, H. Y. Wang, X. Bin Zhong, W. Qi, B. Y. Wang and Q. C. Jiang, *RSC Adv.*, 2014, **4**, 50964–50968.

3 R. Fang, K. Chen, L. Yin, Z. Sun, F. Li and H. M. Cheng, *Adv. Mater.*, 2019, **31**, 1800863.

4 M. Chen, X. Liang, F. Wang, D. Xie, G. Pan and X. Xia, *J. Mater. Chem. A*, 2019, **7**, 6644.

5 P. Canepa, G. Sai Gautam, D. C. Hannah, R. Malik, M. Liu, K. G. Gallagher, K. A. Persson and G. Ceder, *Chem. Rev.*, 2017, **117**, 4287–4341.

6 X. Liang, C. Y. Kwok, F. Lodi-Marzano, Q. Pang, M. Cuisinier, H. Huang, C. J. Hart, D. Houtarde, K. Kaup, H. Sommer, T. Brezesinski, J. Janek and L. F. Nazar, *Adv. Energy Mater.*, 2016, **6**, 1501636.

7 H. Zhao, N. Deng, J. Yan, W. Kang, J. Ju, Y. Ruan, X. Wang, X. Zhuang, Q. Li and B. Cheng, *Chem. Eng. J.*, 2018, **347**, 343–365.

8 X. Liang, C. Minghua, H. Zhu, H. Zhu, X. Cui, J. Yan, Q. Chen, X. Xia and Q. Liu, *J. Mater. Chem. A*, 2020, **8**, 9068.

9 Y. Li, M. Chen, B. Liu, Y. Zhang, X. Liang and X. Xia, *Adv. Energy Mater.*, 2020, 2000927.

10 Z. Chen, D. Chao, M. Chen and Z. Shen, *RSC Adv.*, 2020, **10**, 18776.

11 W. Li, L. Zeng, Y. Wu and Y. Yu, *Sci. China Mater.*, 2016, **59**, 287–321.

12 M. Qi, L. Xinqi, F. Wang, H. Manshu, Y. Jinghua and M. Chen, *J. Alloys Compd.*, 2019, **799**, 345.

13 R. Xu, J. Lu and K. Amine, *Adv. Energy Mater.*, 2015, **5**, 1500408.

14 B. Zhang, F. Kang, J. M. Tarascon and J. K. Kim, *Prog. Mater. Sci.*, 2016, **76**, 319–380.

15 S. Xin, L. Gu, N. H. Zhao, Y. X. Yin, L. J. Zhou, Y. G. Guo and L. J. Wan, *J. Am. Chem. Soc.*, 2012, **134**, 18510–18513.

16 C. Zhang, Y. Xu, M. Zhou, L. Liang, H. Dong, M. Wu, Y. Yang and Y. Lei, *Adv. Funct. Mater.*, 2017, **27**, 1604307.

17 S. Han, X. Pu, X. Li, M. Liu, M. Li, N. Feng, S. Dou and W. Hu, *Electrochim. Acta*, 2017, **241**, 406–413.

18 Y. He, Z. Chang, S. Wu and H. Zhou, *J. Mater. Chem. A*, 2018, **6**, 6155–6182.

19 L. Sun, M. Li, Y. Jiang, W. Kong, K. Jiang, J. Wang and S. Fan, *Nano Lett.*, 2014, **14**, 4044–4049.

20 H. J. Peng, J. Q. Huang and Q. Zhang, *Chem. Soc. Rev.*, 2017, **46**, 5237–5288.

21 Z. Gong, Q. Wu, F. Wang, X. Li, X. Fan, H. Yang and Z. Luo, *RSC Adv.*, 2016, **6**, 37443–37451.

22 Y. C. Jeong, J. H. Kim, S. Nam, C. R. Park and S. J. Yang, *Adv. Funct. Mater.*, 2018, **28**, 1707411.

23 X. Zhou, J. Xie, J. Yang, Y. Zou, J. Tang, S. Wang, L. Ma and Q. Liao, *J. Power Sources*, 2013, **243**, 993–1000.

24 H. Wang, Y. Yang, Y. Liang, J. T. Robinson, Y. Li, A. Jackson, Y. Cui and H. Dai, *Nano Lett.*, 2011, **11**, 2644–2647.

25 Y. Zhong, D. Chao, S. Deng, J. Zhan, R. Y. Fang, Y. Xia, Y. Wang, X. Wang, X. Xia and J. Tu, *Adv. Funct. Mater.*, 2018, **28**, 1706391.

26 L. Xiao, Y. Cao, J. Xiao, B. Schwenzer, M. H. Engelhard, L. V. Saraf, Z. Nie, G. J. Exarhos and J. Liu, *Adv. Mater.*, 2012, **24**, 1176–1181.

27 D. Su, M. Cortie, H. Fan and G. Wang, *Adv. Mater.*, 2017, **29**, 1700587.

28 X. Song, T. Gao, S. Wang, Y. Bao, G. Chen, L. X. Ding and H. Wang, *J. Power Sources*, 2017, **356**, 172–180.

29 Q. Huang, T.-Z. Zhuang, Q. Zhang, H.-J. Peng, C.-M. Chen and F. Wei, *ACS Nano*, 2015, **9**, 3002–3011.